VIP Nonheme Iron Complexes

DOI: 10.1002/anie.200900863

A Synthetic High-Spin Oxoiron(IV) Complex: Generation, Spectroscopic Characterization, and Reactivity**

Jason England, Marlène Martinho, Erik R. Farquhar, Jonathan R. Frisch, Emile L. Bominaar, Eckard Münck,* and Lawrence Que, Jr.**

High-valent oxoferryl intermediates have been proposed as the active oxidants in the catalytic cycles of a wide range of mononuclear non-heme oxygen-activating enzymes.[1] These high-valent species have now been spectroscopically characterized for four enzymes, and were found in all instances to contain high-spin ($S=2$) iron(IV) centers.[2] Contemporaneously, the first examples of the existing family of synthetic nonheme oxoiron(IV) complexes were characterized,[3–5] which are exclusively octahedral and in all but one case exhibit the $S=1$, rather than $S=2$, spin state. Given that DFT suggests higher reactivity for an $S=2$ oxoiron(IV) unit,[6,7] it is perhaps not surprising that there is a scarcity of such complexes. Indeed, the only example to date is $[Fe^{IV}(O)(H_2O)_5]^{2+}$ (**1**), which is generated by treating $[Fe^{II}(H_2O)_6]^{2+}$ with ozone in acidic aqueous solution.[8a] Complex **1** has a $t_{1/2}$ value of only 7 s at 25 °C,[8b] and the aqueous medium limits our options for significantly lengthening its lifetime by working at low temperature ($T<0$ °C). We have consequently sought an alternative approach to obtain an $S=2$ oxoiron(IV) complex.

Consideration of the crystal-field splitting diagram for an octahedral oxoiron(IV) complex reveals that the spin state is determined by the energy gap between the d_{xy} and the $d_{x^2-y^2}$ orbitals.[7] In the $S=1$ complexes reported thus far, this energy gap is larger than the spin-pairing energy. Therefore, weakening the strength of the equatorial ligand field is one strategy to obtain $S=2$ complexes, a principle demonstrated by the tetraaqua ligand set of **1**.[8] An alternative approach is to adopt a trigonal bipyramidal (TBP) geometry, where the d_{xy} and $d_{x^2-y^2}$ orbitals would become degenerate. Thus, a tetradentate tripodal ligand with sufficient steric constraints to enforce local C_{3v} symmetry at the iron(II) center could afford, upon introduction of an axial oxo ligand, a trigonal bipyramidal oxoiron(IV) complex with an $S=2$ ground state. Such a geometry is found for the oxoiron(III) complex of the tris(ureaylato) ligand employed by Borovik and co-workers.[9] This complex was obtained from the reaction of its iron(II) precursor with O_2, and proposed to derive from the reduction of an initially formed oxoiron(IV) species, but to date direct evidence for the latter has not been obtained. TMG_3tren (Figure 1 A) is another example of such a ligand.[10] This ligand has recently found use in the successful stabilization of a superoxocopper(II) complex and its subsequent structural characterization.[11] Furthermore, the high level of steric encumbrance provided by TMG_3tren should inhibit intermo-

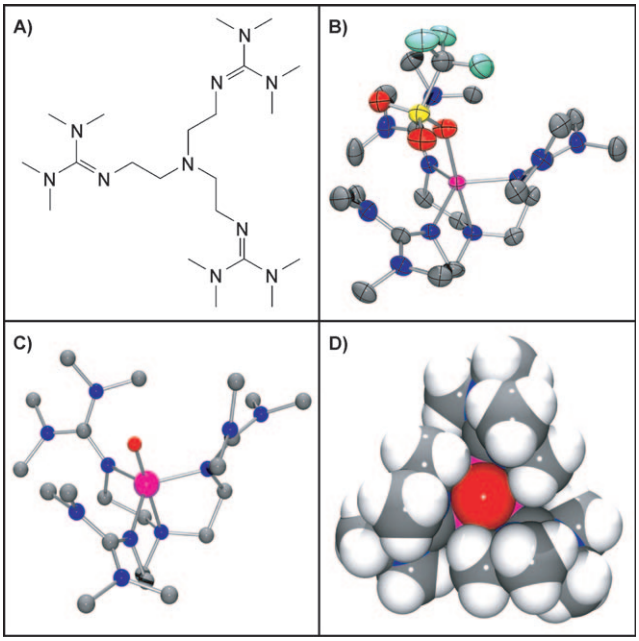

Figure 1. A) Schematic structure of the TMG_3tren ligand. B) Solid-state structure of $[Fe^{II}(TMG_3tren)(OTf)]^+$ (**2**; OTf = trifluoromethanesulfonate), with ellipsoids shown at 50% probability. Hydrogen atoms have been omitted for clarity. Selected bond distances [Å]: Fe–O, 2.156(2); Fe–N_{axial}, 2.118(3); Fe–$N_{guanidine}$(ave), 2.094. C) Ball-and-stick and D) space-filling models of the geometry-optimized structure of **3** calculated by DFT. Selected bond distances [Å]: Fe=O, 1.648; Fe–N_{axial}, 2.121; Fe–$N_{guanidine}$(ave), 2.034. Atom color scheme: C, gray; N, blue, O, red; S, yellow; F, light blue; Fe, magenta.

[*] Dr. M. Martinho, Prof. Dr. E. L. Bominaar, Prof. Dr. E. Münck
Department of Chemistry, Carnegie Mellon University
Pittsburgh, PA 15213 (USA)
E-mail: eb7g@andrew.cmu.edu
emunck@cmu.edu
Dr. J. England, E. R. Farquhar, J. R. Frisch, Prof. Dr. L. Que, Jr.
Department of Chemistry and Center for Metals in Biocatalysis
University of Minnesota
207 Pleasant St. SE, Minneapolis, MN 55455 (USA)
Fax: (+1) 612-624-7029
E-mail: larryque@umn.edu

[**] This work was supported by grants from the NIH (GM-33162 to L.Q. and EB-001475 to E.M.) and the NSF (CHE070073 to E.L.B. through TeraGrid resources provided by the NCSA). X-ray crystallographic data collection and structure elucidation were performed by Dr. Victor G. Young, Jr. at the X-Ray Crystallographic Laboratory, Department of Chemistry, University of Minnesota. XAS data were collected on beamline X3B at the National Synchrotron Radiation Light Source and beamline 7-3 at the Stanford Synchrotron Lightsource, both of which are supported by the U.S. DOE and NIH.

Supporting information for this article is available on the WWW under http://dx.doi.org/10.1002/anie.200900863.

lecular decay processes, thereby stabilizing the highly reactive Fe^{IV}=O unit.

The combination of equimolar amounts of TMG_3tren and $[Fe^{II}(OTf)_2(CH_3CN)_2]$ in THF afforded $[Fe^{II}(TMG_3tren)(OTf)](OTf)$ (**2**), whose crystal structure (Figure 1B)[12] exhibited the desired TBP geometry ($\tau = 0.96$[13]). Reaction of **2** in CH_3CN with one equivalent of 2-(*tert*-butylsulfonyl)-iodosylbenzene ($tBuSO_2C_6H_4IO$)[14] led to the formation of an orange complex **3** ($t_{1/2} = 4.3$ h at $-30\,^\circ C$; $t_{1/2} \approx 30$ s at $25\,^\circ C$) with absorption maxima λ_{max} (ε_{max}) centered at 400 (9800), 825 (260), and 866 (250) nm (Figure 2). The electrospray mass

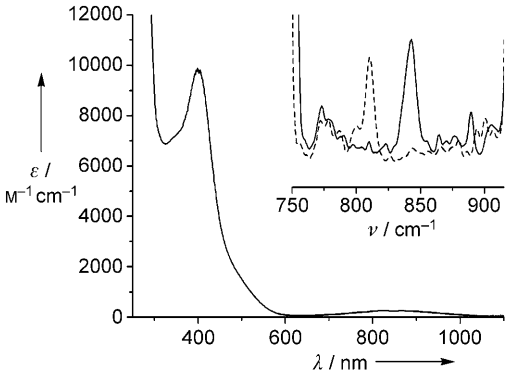

Figure 2. Electronic spectrum of **3** in CH_3CN solution. Inset: resonance Raman spectra ($\lambda_{ex} = 514.5$ nm, power = 10 mW) of [^{16}O]-**3** (solid line) and [^{18}O]-**3** (dashed line) recorded in frozen CH_3CN solution.

spectrum of **3** exhibited signals at $m/z = 661.3$ and 256.2, with isotope distribution patterns consistent with their respective formulation as $\{[Fe^{IV}(O)(TMG_3tren)](OTf)\}^+$ and $[Fe^{IV}(O)(TMG_3tren)]^{2+}$ (see Figures S1 and S2 in the Supporting Information). The presence of an Fe=O unit in **3** was confirmed by resonance Raman spectroscopy, which revealed a vibration at 843 cm^{-1} that shifted to 810 cm^{-1} upon ^{18}O-labeling of **3** (Figure 2, inset). This vibrational frequency and isotope shift ($\Delta\nu_{theor} \approx 37$ cm^{-1}) are both consistent with its assignment as ν(Fe=O). Furthermore, the ^{19}F NMR spectrum of **3** displayed a single resonance at $\delta = -79.9$ ppm, which corresponds to free triflate. This observation, coupled with the fact that **3** exhibits the same UV/Vis spectrum in both coordinating (CH_3CN) and noncoordinating (CH_2Cl_2) solvents, indicates that no exogeneous ligands bind to the iron center and that, by extension, the five-coordinate geometry found in **2** is retained in **3**, thus leading us to formulate the latter as $[Fe^{IV}(O)(TMG_3tren)]^{2+}$.

Mössbauer spectroscopy demonstrates that **3** has an $S = 2$ iron(IV) center. The zero-field spectrum (Figure 3A) exhibits a doublet with a quadrupole splitting $\Delta E_Q = -0.29$ mm s^{-1} and isomer shift $\delta = 0.09$ mm s^{-1}. The observation of a doublet in the spectrum at 4.2 K indicates that **3** has integer electronic spin. The δ value is strongly indicative of an iron(IV) complex, and although the value of δ is distinctly lower than those for **1** (0.38 mm s^{-1})[8a] and TauD intermediate **J** (TauD-**J**; 0.30 mm s^{-1}),[15c] it is similar to that of the Fe^{IV} site of $[Fe^{IV}(O)(6\text{-}Me_3tpa)(\mu\text{-}O)Fe^{III}(6\text{-}Me_3tpa)(H_2O)]$ (0.10 mm s^{-1}; 6-Me_3-tpa = tris(6-methylpyridyl-2-methyl)amine),[17] reflecting the nitrogen-rich ligand environment of **3**. Approximately 88% of the Fe in the sample belongs to **3**. A minor high-spin Fe^{III} contaminant accounts for the remaining absorption (see Figure S3 in the Supporting Information). The spectra of **3** exhibit paramagnetic hyperfine structure in applied magnetic fields. Fitting these spectra with an $S = 2$ spin Hamiltonian yields a parameter set that compares well with other high-spin oxoiron(IV) systems (Table 1). In contrast, analysis of the data by assuming an $S = 1$ center yields an unacceptable ***A*** tensor, with $A_{iso} = (A_x + A_y + A_z)/3 \approx -29.0$ T, which is nearly twice as large as A_{iso} values reported for $S = 1$ complexes.[4,5,16,18] Moreover, the spin-dipolar part of the ***A*** tensor, ($\boldsymbol{A} - A_{iso}$), would be about four times smaller than observed for $S = 1$ Fe^{IV}=O complexes.

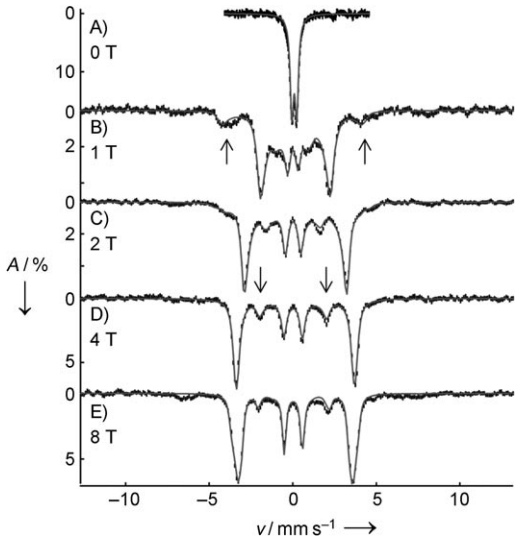

Figure 3. Mössbauer spectra of **3** in CH_3CN recorded at 4.2 K in parallel applied magnetic fields *B* as indicated. Downward arrows indicate nuclear $\Delta m = 0$ transitions of the $M_S = 0$ ground-state spectrum. Upward arrows mark outer absorption features of the spectrum associated with the $M_S = -1$ excited state. Solid lines are spectral simulations using the parameters listed in Table 1 with the $S = 2$ spin Hamiltonian $H = D(S_{z^2} - 2) + E(S_{x^2} - S_{y^2}) + 2\beta \boldsymbol{S}\cdot\boldsymbol{B} + \boldsymbol{S}\cdot\boldsymbol{A}\cdot\boldsymbol{I} - g_n\beta_n \boldsymbol{B}\cdot\boldsymbol{I} + H_Q$. In spectra (B), (C), and (D) a high-spin Fe^{III} impurity, representing 12% of the iron, has been subtracted from the raw data. In trace (E), this impurity has not been subtracted and exhibits weak absorption bands at ca. −6.5 and +7 mm s^{-1}.

The Fe K-edge X-ray absorption spectrum of **3** reveals an edge energy of 7123.2 eV (versus 7121.1 eV for **2**) and a pre-edge peak assigned to 1s→3d transitions with an area of 27 units (Figure 4, top), both features being within the range of values found for the synthetic Fe^{IV}=O complexes previously studied.[16,19] In contrast to the pre-edge features of existing $S = 1$ complexes, which can be modeled with a single Gaussian, the pre-edge region of **3** contains two discernible features at 7113.8 and 7115.6 eV that have areas of 24 and 3 units, respectively (see Figure S4 and Table S1 in the Supporting Information). This phenomenon was predicted in a recent DFT study,[20a] and was rationalized in terms of a splitting of the α and β d_{z^2} orbitals by spin polarization, which is expected to be significantly larger in the $S = 2$ case.[20] EXAFS analysis of **3** (Figure 4, bottom) yields a best-fit plot (see Table S2 in the Supporting Information) with an O/N

Table 1: Spectroscopic parameters of selected oxoiron(IV) complexes.

Complex	S	λ_{max} [nm]	$\nu_{Fe=O}$ [cm^{-1}]	D [cm^{-1}]	E/D	$A_{x,y,z}/g_n\beta_n$ [T]	ΔE_Q [$mm\,s^{-1}$]	η	δ [$mm\,s^{-1}$]	E_0 [eV]	Pre-edge area
3 (exp)	2	400	843	5.0(3)	0.02(1)	−15.5(4), −14.8(4), −28.0(8)	−0.29(3)	0	0.09(1)	7123.2	27
3 (DFT)[a]	2	–	–	–	–	−15, −15, −27.6	−0.49	0.02	0.11	–	–
TauD-**J**[b]	2	318	821	10.5	0.01	−18.4, −17.6, −31.0	−0.9	0	0.30	7123.8[d]	not reported
1[c]	2	320	–	9.7	0	−20.3, −20.3, nd	−0.33	0	0.38	7126	60-70
4[c]	1	820	834	29	0	−22.6, −18.3, −2.9	1.24	0.5	0.17	7124.5	32.8

[a] The ***A*** tensor was calculated by taking the experimentally determined $A_{iso} = -19.4$ T and adding the spin-dipolar term obtained from DFT. [b] Data from Refs [2a, 15]. [c] **1** = $[Fe^{IV}(O)(OH_2)_5]^{2+}$ from Ref. [8]; **4** = $[Fe^{IV}(O)(TMC)(NCCH_3)]^{2+}$ (TMC = 1,4,8,11-tetramethylcyclam) from Refs. [4, 16]. [d] Assuming an Fe foil reference E of 7112.0 eV.

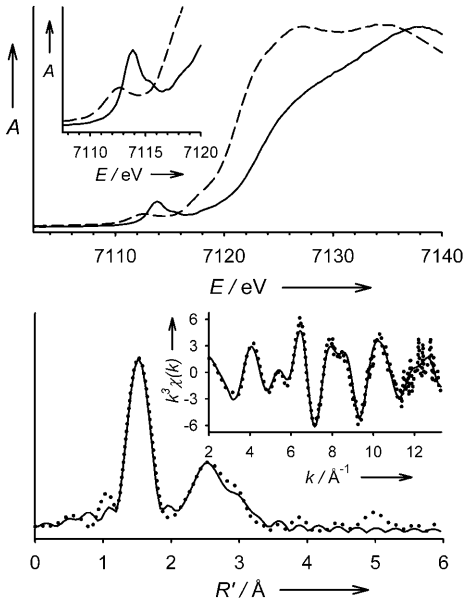

Figure 4. Top: X-ray absorption edge spectra of **2** (-----) and **3** (——). The inset shows an expansion of the pre-edge region. Bottom: Fe K-edge unfiltered EXAFS data ($k^3\chi(k)$, inset) and the corresponding Fourier transform of **3**. Experimental data are shown with dotted lines and fits with solid lines. See the Supporting Information for further details of the EXAFS analysis.

scatterer at 1.65 Å (assigned to the Fe=O unit) and a further shell of 4 O/N scatterers at 1.99 Å (corresponding to the N donors of the supporting ligand). This Fe=O distance is essentially the same as that found crystallographically for other oxoiron(IV) complexes.[4,18,21]

DFT calculations performed on **3** further support our $S = 2$ spin-state assignment. Geometry optimization yields a structure with C_3 symmetry (Figure 1C) and an Fe=O bond length of 1.648 Å, which is in close agreement with that obtained from the EXAFS analysis. In contrast, the Fe–N_{ave} bond length of 2.055 Å obtained from DFT is significantly longer than that found by EXAFS. Complex **3** has a ^5A ground state with the four d electrons in two half-filled E levels (see Table S3 in the Supporting Information), with the lowest $S = 1$ and $S = 0$ configurations calculated to be about 10000 cm^{-1} and 12000 cm^{-1}, respectively, above the $S = 2$ ground state. Notably, the calculated Mössbauer parameters (ΔE_Q, δ, and the spin-dipolar contribution to the ***A*** tensor) are in excellent agreement with the experimental data (Table 1). The small value for ΔE_Q results from cancellation of opposing valence and ligand contributions, the latter arising from the donation of electron density from the oxo ligand into the vacant E{d_{xz}, d_{yz}} and empty A{d_{z^2}} orbitals of the iron center. Lastly, the calculated spin populations at the iron center and the oxo group are +3.08 and +0.64, respectively, similar to the results obtained for **1** and TauD-**J**.[8a,15c]

The oxidative reactivity of **3** has been investigated with several substrates, and the second-order rate constants derived from these studies in CH_3CN solution at −30 °C are listed in Table 2, together with those of the well-studied $S = 1$ complexes $[Fe^{IV}(O)(TMC)(CH_3CN)]^{2+}$ (**4**)[4,16,22] and $[Fe^{IV}(O)(N4Py)]^{2+}$ (**5**; N4Py = bis(2-pyridylmethyl)bis(2-pyridyl)methylamine).[21,23] Complex **3** acts as a stoichiometric oxo-transfer agent to PPh_3, but behaves as a $1e^-$ oxidant in reactions with dihydroanthracene (DHA) and 1,4-cyclohexadiene (CHD), with two equivalents of **3** yielding one equivalent of anthracene and benzene, respectively. In general, **3** is a more active oxidant than **4**, but comparable to **5**. Surprisingly, **3** oxidizes DHA 13 times more slowly than CHD, despite there being no significant difference in the oxidation rates of these two substrates by either **4** or **5**. Since DHA and CHD have similar C–H bond dissociation energies,[24] the large rate difference observed for **3** suggests that the TMG_3tren ligand impedes access of the bulkier DHA to the Fe=O unit (Figure 1D and Figure S5 in the Supporting Information). Such a sterically derived mitigation of reactivity has been observed for other systems with tetramethylguanidinyl ligands.[25] Lastly, the use of [D_4]DHA as the substrate for **3** afforded a kinetic isotope effect (KIE) of 18, which is above the semiclassical limit of 7. Thus, as for the $S = 2$ oxoferryl enzymatic intermediates[1] and the $S = 1$ complexes **4** and **5**,[22,23] there appears to be a significant contribution

Table 2: Second-order rate constants (k_2) for oxidation reactions of Fe^{IV}=O complexes.

Complex	k_2 [$M^{-1}s^{-1}$] in CH_3CN at −30 °C		
	PPh_3	DHA	CHD
3	1.1	0.090	1.2
4	0.22	0.016	0.018
5	1.5	2.0	1.3

from hydrogen atom tunneling in the cleavage of the C–H bond by **3**.

Herein we have described the high-yield synthesis of an $S=2$ oxoiron(IV) complex that has been characterized fully by spectroscopy. Complex **3** resembles TauD-**J** in several respects (Table 1). Both **3** and TauD-**J** exhibit a near-UV charge-transfer band that is likely to be associated with an oxo-to-iron(IV) charge-transfer transition, as excitation into these bands results in the observation of resonance-enhanced Fe=O vibrations.[15a] The charge-transfer band of **3** is red-shifted relative to that of TauD-**J**. This observation is in line with the greater Lewis acidity expected for an oxoiron(IV) unit supported by the neutral TMG_3tren ligand, instead of the dianionic bis(carboxylato)-containing coordination sphere of TauD-**J**.[2a,15c] Differences in the coordination environment are also reflected in the Mössbauer parameters. Interestingly, **3** exhibits an oxidative efficacy that is merely comparable to that of the $S=1$ complex **5** (Table 2), rather than exceeding it. This finding appears to belie the prevailing DFT-derived consensus that the $S=2$ manifold is inherently more reactive than the corresponding $S=1$ state.[6,7] This attenuation in the reactivity of **3** most likely derives from the protection of the high-spin oxoiron(IV) moiety afforded by the sterically bulky TMG_3tren ligand, a design strategy we have successfully employed here to attain the elusive $S=2$ spin state. Further ligand tuning may allow access to more-reactive $S=2$ oxoiron(IV) model complexes that might provide invaluable insight into the inherent reactivity and spectroscopic properties of these key biologically relevant entities.

Experimental Section

2: A solution of TMG_3tren (0.55 g, 1.25 mmol) in THF (10 mL) was added to a Schlenk flask charged with $[Fe(OTf)_2(CH_3CN)_2]$ (0.54 g, 1.25 mmol), and the resultant mixture stirred overnight. The cream precipitate obtained was isolated by filtration, washed with THF (3 × 5 mL) and diethyl ether (2 × 15 mL), and dried under vacuum to give an off-white powder (0.97 g, 93%) that analyzed as a monoacetonitrile adduct. Elemental analysis calcd for $C_{25}H_{51}F_6FeN_{11}O_6S_2$: C 35.93, H 6.15, N 18.44; found: C 35.89, H 6.21, N 18.24. The acetonitrile-free compound was obtained as a pale yellow crystalline solid (0.84 g, 85% overall) by vapor diffusion of diethyl ether into a concentrated dichloromethane solution of the iron(II) complex. ^{1}H NMR (300 MHz, CD_3CN, all signals appear as broad singlets): $\delta=213.2$ (3H, CH_2), 86.7 (3H, CH_2), 61.7 (3H, CH_2), 34.3 (9H, NMe), 20.9 (9H, NMe), 9.9 (9H, NMe), 1.3 (3H, CH_2), −13.6 ppm (9H, NMe). MS (+ESI): m/z 645.1 $[(M-OTf)^+]$, 248.1 $[\{M-(OTf)_2\}^{2+}]$. Elemetal analysis calcd for $C_{23}H_{48}F_6FeN_{10}O_6S_2$: C,34.76, H 6.09, N 17.63; found: C 34.67, H 6.19, N 17.51.

3(OTf)$_2$: Solutions of the orange complex **3** were obtained by treatment of a solution of **2** in CH_3CN or CH_2Cl_2 with a solution of one equivalent of tBuSO$_2$C$_6$H$_4$IO[14] in CH_2Cl_2. Solutions of oxidant up to a concentration of 60 mM were routinely used.

Received: February 13, 2009
Published online: April 16, 2009

Keywords: bioinorganic chemistry · enzyme models · high-valent compounds · iron · nonheme iron complexes

[1] C. Krebs, D. Galonic Fujimori, C. T. Walsh, J. M. Bollinger, Jr., *Acc. Chem. Res.* **2007**, *40*, 484.
[2] a) J. C. Price, E. W. Barr, B. Tirupati, J. M. Bollinger, Jr., C. Krebs, *Biochemistry* **2003**, *42*, 7497; b) L. M. Hoffart, E. W. Barr, R. B. Guyer, J. M. Bollinger, Jr., C. Krebs, *Proc. Natl. Acad. Sci. USA* **2006**, *103*, 14738; c) B. E. Eser, E. W. Barr, P. A. Frantom, L. Saleh, J. M. Bollinger, Jr., C. Krebs, P. F. Fitzpatrick, *J. Am. Chem. Soc.* **2007**, *129*, 11334; d) D. P. Galonic, E. W. Barr, C. T. Walsh, J. M. Bollinger, Jr., C. Krebs, *Nat. Chem. Biol.* **2006**, *3*, 113.
[3] L. Que, Jr., *Acc. Chem. Res.* **2007**, *40*, 493.
[4] J.-U. Rohde, J.-H. In, M. H. Lim, W. W. Brennessel, M. R. Bukowski, A. Stubna, E. Münck, W. Nam, L. Que, Jr., *Science* **2003**, *299*, 1037.
[5] M. H. Lim, J.-U. Rohde, A. Stubna, M. R. Bukowski, M. Costas, R. Y. N. Ho, E. Münck, W. Nam, L. Que, Jr., *Proc. Natl. Acad. Sci. USA* **2003**, *100*, 3665.
[6] a) H. Hirao, D. Kumar, L. Que, Jr., S. Shaik, *J. Am. Chem. Soc.* **2006**, *128*, 8590; b) L. Bernasconi, M. J. Louwerse, E. J. Baerends, *Eur. J. Inorg. Chem.* **2007**, 3023.
[7] A. Decker, J.-U. Rohde, E. J. Klinker, S. D. Wong, L. Que, Jr., E. I. Solomon, *J. Am. Chem. Soc.* **2007**, *129*, 15983.
[8] a) O. Pestovsky, S. Stoian, E. L. Bominaar, X. Shan, E. Münck, L. Que, Jr., A. Bakac, *Angew. Chem.* **2005**, *117*, 7031; *Angew. Chem. Int. Ed.* **2005**, *44*, 6871; b) O. Pestovsky, A. Bakac, *J. Am. Chem. Soc.* **2004**, *126*, 13757.
[9] C. E. MacBeth, A. P. Golombek, V. G. Young, Jr., C. Yang, K. Kuczera, M. P. Hendrich, A. S. Borovik, *Science* **2000**, *289*, 938.
[10] H. Wittmann, V. Raab, A. Schorm, J. Plackmeyer, J. Sundermeyer, *Eur. J. Inorg. Chem.* **2001**, 1937.
[11] C. Würtele, E. Gaoutchenova, K. Harms, M. C. Holthausen, J. Sundermeyer, S. Schindler, *Angew. Chem.* **2006**, *118*, 3951; *Angew. Chem. Int. Ed.* **2006**, *45*, 3867.
[12] Single-crystal structure and refinement data for **2**: $C_{23}H_{48}F_6FeN_{10}O_6S_2$, $M_w=794.68$, monoclinic, space group $P2_1/c$, $a=12.6127(17)$, $b=15.273(2)$, $c=18.880(3)$ Å, $\alpha=90$, $\beta=94.573(2)$, $\gamma=90°$, $V=3625.3(8)$ Å^3, $Z=4$, $\rho_{calcd}=1.456$ Mg m^{-3}, $Mo_{K\alpha}$ radiation ($\lambda=0.71073$ Å, $\mu=0.612$ mm^{-1}), $T=173(2)$ K. A total of 7417 ($R_{int}=0.0353$) independent reflections with $2\theta<26.39°$ were collected. The resulting parameters were refined to converge at $R_1=0.0465$ ($I>2\theta$) for 518 parameters on 7417 independent reflections ($wR_2=0.1390$). Max./min. residual electron density 0.977/−0.493 e Å^{-3}; GOF = 1.114. Further experimental details are provided in the Supporting Information. CCDC 714035 contains the supplementary crystallographic data for this paper. These data can be obtained free of charge from The Cambridge Crystallographic Data Centre via www.ccdc.cam.ac.uk/data_request/cif..
[13] A. W. Addison, T. N. Rao, J. Reedijk, J. Van Rijn, G. C. Verschoor, *J. Chem. Soc. Dalton Trans.* **1984**, 1349.
[14] D. Macikenas, E. Skrzypczak-Jankun, J. D. Protasiewicz, *J. Am. Chem. Soc.* **1999**, *121*, 7164.
[15] a) D. A. Proshlyakov, T. F. Henshaw, G. R. Monterosso, M. J. Ryle, R. P. Hausinger, *J. Am. Chem. Soc.* **2004**, *126*, 1022; b) P. J. Riggs-Gelasco, J. C. Price, R. B. Guyer, J. H. Brehm, E. W. Barr, J. M. Bollinger, Jr., C. Krebs, *J. Am. Chem. Soc.* **2004**, *126*, 8108; c) S. Sinnecker, N. Svensen, E. W. Barr, S. Ye, J. M. Bollinger, Jr., F. Neese, C. Krebs, *J. Am. Chem. Soc.* **2007**, *129*, 6168.
[16] T. A. Jackson, J.-U. Rohde, M. S. Seo, C. V. Sastri, R. DeHont, A. Stubna, T. Ohta, T. Kitagawa, E. Münck, W. Nam, L. Que, *J. Am. Chem. Soc.* **2008**, *130*, 12394.
[17] H. Zheng, S. J. Yoo, E. Münck, L. Que, Jr., *J. Am. Chem. Soc.* **2000**, *122*, 3789.
[18] A. Thibon, J. England, M. Martinho, V. G. Young, J. R. Frisch, R. Guillot, J.-J. Girerd, E. Münck, L. Que, Jr., F. Banse, *Angew. Chem.* **2008**, *120*, 7172; *Angew. Chem. Int. Ed.* **2008**, *47*, 7064.

[19] J.-U. Rohde, S. Torelli, X. Shan, M. H. Lim, E. J. Klinker, J. Kaizer, K. Chen, W. Nam, L. Que, Jr., *J. Am. Chem. Soc.* **2004**, *126*, 16750.

[20] a) J. F. Berry, S. DeBeer George, F. Neese, *Phys. Chem. Chem. Phys.* **2008**, *10*, 4361; b) A. Decker, M. D. Clay, E I. Solomon, *J. Inorg. Biochem.* **2006**, *100*, 697.

[21] E. J. Klinker, J. Kaizer, W. W. Brennessel, N. L. Woodrum, C. J. Cramer, L. Que, Jr., *Angew. Chem.* **2005**, *117*, 3756; *Angew. Chem. Int. Ed.* **2005**, *44*, 3690.

[22] S. V. Chivukula, J. Lee, K. Oh, Y. J. Lee, J. Lee, T. A. Jackson, K. Ray, H. Hirao, W. Shin, J. A. Halfen, J. Kim, L. Que, Jr., S. Shaik, W. Nam, *Proc. Natl. Acad. Sci. USA* **2007**, *104*, 19181.

[23] J. Kaizer, E. J. Klinker, N. Y. Oh, J.-U. Rohde, W. J. Song, A. Stubna, J. Kim, E. Münck, W. Nam, L. Que, Jr., *J. Am. Chem. Soc.* **2004**, *126*, 472.

[24] Y.-R. Luo, *Comprehensive Handbook of Chemical Bond Energies*, CRC, Boca Raton, **2007**.

[25] S. Herres-Pawlis, P. Verma, R. Haase, P. Kang, C. T. Lyons, E. C. Wasinger, U. Floerke, G. Henkel, T. D. P. Stack, *J. Am. Chem. Soc.* **2009**, *131*, 1154.

